COMMUNICATION

Two-step synthesis of Fe_2O_3 and Co_3O_4 nanoparticles: towards a general method for synthesizing nanocrystalline metal oxides with high surface area and thermal stability†

Junjiang Zhu,*[ab] Xiaoying Ouyang,[c] Ming-Yung Lee,[b] Ryan C. Davis,[c] Susannah L. Scott,*[bc] Anna Fischer[a] and Arne Thomas[a]

A simple, two-step method using activated carbon (AC) as a support/scaffold was developed to synthesize metal oxide nanocrystalline materials (NCMs). In the first step, metal nitrate precursors were deposited by wet impregnation onto the AC, then heated in argon at 350 °C to immobilize the metal oxides. In the second step, the AC was removed by calcination in air at 500 °C, to obtain the unsupported metal oxide NCMs. Characterization by N_2-sorption isotherms, TGA, XPS and EXAFS reveals that the metal oxide particles are crystalline and nanometre-sized, with surface areas up to 148 $m^2 g^{-1}$. Moreover, the TEM images show particle sizes in the range 5–10 nm, even after calcination at 500 °C for 2 h. Their thermal stability and high surface areas, together with the nanometre-sized structures, make them promising materials for catalytic applications (*e.g.*, CO oxidation).

Introduction

Nanocrystalline materials (NCMs) have attracted much attention in recent years because of a wide variety of potential applications, including catalysis, optics and chemical sensors.[1–8] In catalysis, it is generally believed that, in addition to enhanced surface areas, NCMs often display interesting and unexpected properties that are qualitatively different from those of the corresponding bulk materials, or of the atomic or molecular species from which they are derived.[9] One well-known example is the use of gold for low temperature CO oxidation: bulk gold shows no activity, while gold nanoparticles (NPs) show high reactivity even at 77 K.[10–12]

Defining and understanding the origin of the novel properties of NCMs has stimulated much research, and consequently, methods to prepare them have been extensively reported, both for metal oxides[13–18] and for noble metals.[19–23] Compared to the preparation of noble metal-based materials, the synthesis of metal oxide NCMs can be more complex, because some metals are very reactive toward oxygen, and agglomeration of oxide NPs occurs readily at moderate temperatures. Straightforward, versatile routes for the synthesis of thermally stable metal oxide NCMs are therefore of considerable practical interest.

Activated carbon (AC) has long been recognized as a good support for both noble and base metal catalysts, due to its microporosity, multifunctional surface groups and high surface area.[24–28] For a noble metal such as gold, Prati *et al.*[29,30] found that when Au^{3+} is first reduced to Au^0 in the presence of polyvinyl alcohol (PVA) and then immobilized on AC, small gold particles ($\sim$6 nm) can be obtained after removing the PVA at 350 °C. We found that very small Co_3O_4·NPs ($\sim$5 nm) are obtained when a metal nitrate-impregnated AC is heated in argon at 350 °C.[31,32] AC has also been used to prepare unsupported metal oxides with high surface areas and designed structures.[33–39] For example, Schüth *et al.*[37] obtained metal oxides with surface areas ranging from 50 to 200 $m^2 g^{-1}$ by calcining metal nitrates deposited on AC in air at 450–800 °C. They reported better results for some metals (*e.g.*, Cu) by heating in the presence of a limited amount of air, and suggested that slowing metal nitrate-catalyzed AC combustion reduces particle sintering. These observations inspired us to prepare metal oxide NPs using a prior immobilization step. By removing the AC scaffold in air in a subsequent step, we hoped to obtain unsupported, metal oxide NCMs with small particle sizes and high surface areas.

Results and discussion

For preparation of the metal oxide NCMs, a metal nitrate was first deposited by wet impregnation onto a microporous AC. The resulting material (denoted M/AC-1, where M is Co, Fe) was then dried and heated in a stream of argon at 350 °C, to generate and immobilize the metal oxide NPs on AC, denoted M/AC-2. Subsequently, the solid was allowed to cool to room temperature and heated again to 500 °C in air for 2 h, to remove the AC scaffold and recover the unsupported, nanocrystalline metal oxide.

[a] Department of Chemistry, Technical University of Berlin, Englische Straße 20, 10587, Berlin, Germany. E-mail: ciaczjj@gmail.com (J. Zhu)
[b] Department of Chemical Engineering, University of California, Santa Barbara, 10 Mesa Road, Santa Barbara, CA, 93106-5080, USA. E-mail: sscott@engineering.ucsb.edu (S. L. Scott)
[c] Department of Chemistry & Biochemistry, University of California, Santa Barbara, 10 Mesa Road, Santa Barbara, CA, 93106-9510, USA
† Electronic supplementary information (ESI) available: Experimental details, additional N_2-sorption isotherms, XRD, XPS, TGA, and TEM images of the metal oxides before and after their use as catalysts. See DOI: 10.1039/c1ra00552a

Fig. 1(A) and (B) show the thermal behavior of the materials at each stage during their synthesis, as monitored by thermogravimetric analysis (TGA). AC is thermally stable up to approx. 560 °C in oxygen (see Fig. S1†), and as expected no appreciable weight loss was observed for the AC at $T < 500$ °C in the inert atmosphere (curve "a"). Co/AC-1 (curve "b") shows a stepwise weight loss during thermal treatment in the inert atmosphere. Stage (1), at $T < 120$ °C, is ascribed to loss of water and other adventitious adsorbates acquired during sample storage; stage (2), at $120 < T < 180$ °C, is caused by transformation of $[Co(OH_2)_6](NO_3)_2$ introduced in the impregnation step to $[Co_3[NO_3]_2(OH)_4]$; stage (3), at $180 < T < 240$ °C, corresponds to the decomposition of $[Co_3[NO_3]_2(OH)_4]$ to a cobalt oxide (Co_3O_4).[31] These transformations are similar to those observed previously in the synthesis of supported NiO nanoparticles.[2] After formation of the supported metal oxide, the AC scaffold was removed in O_2, as represented by curve "c". It shows that (i) no appreciable weight loss occurs at $120 < T < 240$ °C, confirming that most of the nitrate was removed during the first thermal treatment step; and (ii) AC is fully removed at $T < 400$ °C, suggesting that the final product calcined at 500 °C should not contain any residual AC scaffold. This is further evidenced by the TGA behavior of the product (curve "d"), which shows a weight loss of less than 5% at $T = 510$ °C in O_2. Similar changes were observed for M = Fe, except that the temperature required for complete removal of the AC scaffold (curve "f") was slightly higher than 500 °C. Nevertheless, the minor weight loss observed for Fe_2O_3 (<5%, curve "g") suggests that AC had been completely removed from the final product.

Thus the characterization and reactivity results below are considered to pertain exclusively to the unsupported metal oxides. By comparing the weight losses of samples Co/AC-2 and Fe/AC-2 with that of the unmodified AC, we estimate the loadings of Co_3O_4 and Fe_2O_3 prior to calcination to be 22 and 14 wt%, respectively.

Results obtained by X-ray photoelectron spectroscopy (XPS) confirm our conclusions based on TGA measurements. Fig. 1(C) shows that the N 1s signal is no longer present after the sample has been heated in Ar at 350 °C for 2 h, indicating that the metal nitrate decomposes completely to the metal oxide. Also, the intensity of the C 1s signal is strongly attenuated in the final product compared to the sample prior to calcination, indicating that AC is indeed removed in the second step. (The weak residual C 1s signal observed for the metal oxide arises due to the carbon tape used to hold the sample in place.) The small amount of S is presumably due to impurities in the AC scaffold: *ca.* 11 wt% non-combustible impurities are present according to the TGA of AC recorded in air, and may include S, Al, Si, *etc.*

In the powder X-ray diffraction (XRD) patterns of the metal oxide NCMs, the reflections are very weak and broad (see Fig. S3†), complicating their assignment and implying that the particle sizes are very small. This agrees with observations made previously for AC-supported cobalt oxide (Co_3O_4/AC), in which peak intensities were very low due to the small particle size (*ca.* 5 nm).[31] Thus, we infer that the metal oxide NPs formed during the first preparation step do not grow appreciably when the AC support is removed. Low peak intensities could also indicate that the metal oxides are in an amorphous state, however, this possibility can be excluded since well-resolved lattice fringes are observed in the high resolution transmission electron microscopy (HR-TEM) images (Fig. 2(C)), typical of a crystalline structure. Consequently, phase assignment was carried out using extended X-ray absorption fine structure (EXAFS). The results shown in Fig. 1(D) and (E) are consistent with spinel Co_3O_4[40] and α-Fe_2O_3[41] for the cobalt and iron oxides, respectively. The ratio of peak heights for the M–O and M–M scattering paths is a reflection of the particle size.[42] We estimate that the Fe_2O_3 particles are in the range 2–10 nm, by comparison to
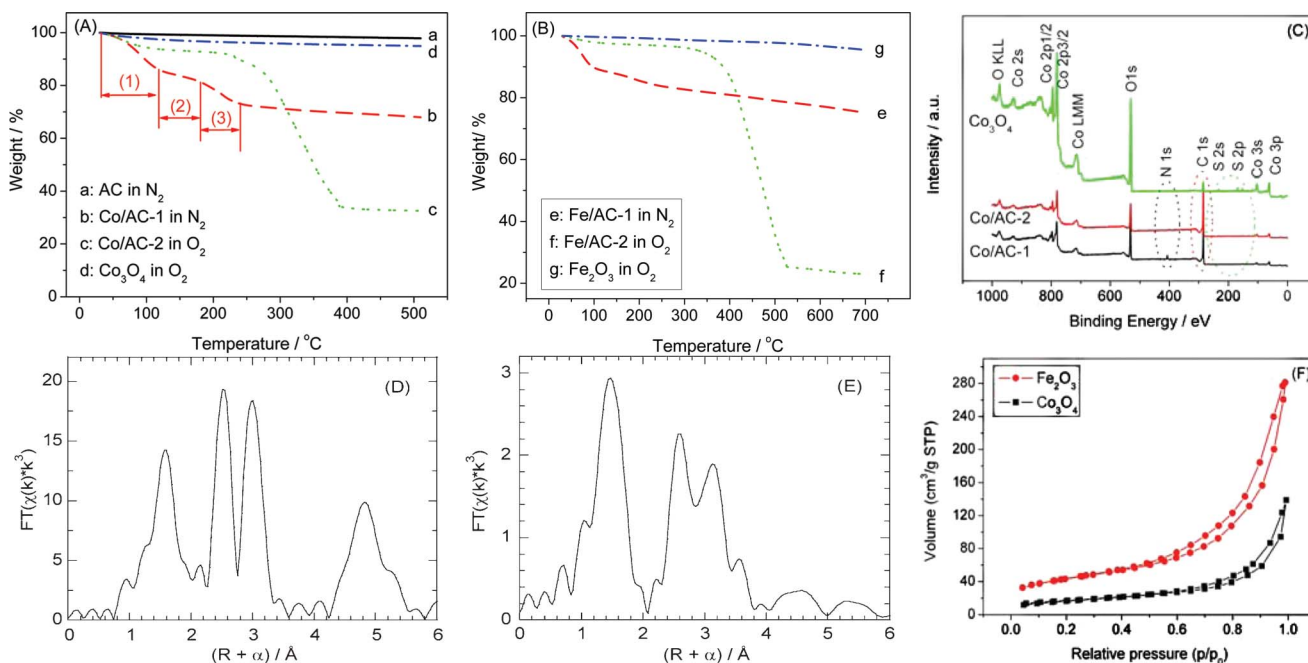
Fig. 1 TGA curves for Co-containing (A) and Fe-containing samples (B), as well as XPS spectra for the Co-containing samples (C), before and after removal of the AC scaffold; *R*-space EXAFS at the Co K-edge for unsupported Co_3O_4_NSMs (D), and at the Fe K-edge for unsupported Fe_2O_3_NSMs (E), and N_2-sorption isotherms for Co_3O_4_NSMs and Fe_2O_3_NSMs (F). "M/AC-1" and "M/AC-2" represent materials before and after treatment in the inert atmosphere, respectively.
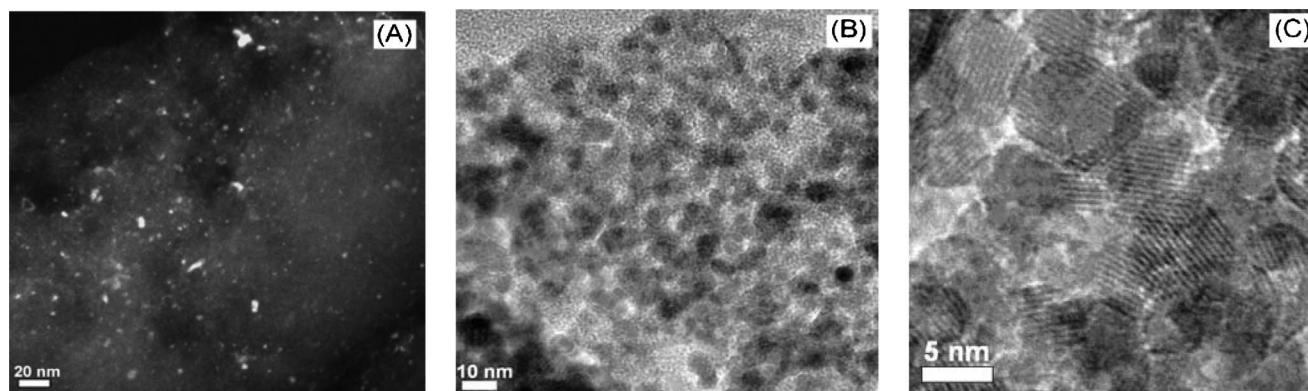
Fig. 2 HR-TEM images for AC-supported $Co_3O_4 \cdot$NCMs, obtained in the first step (A), dark-field; and unsupported $Co_3O_4 \cdot$NCMs obtained in the second step (B), (C), bright-field. Note: for results involving Fe_2O_3, see the ESI.†

spectra reported by Kitagami et al.[43] These observations confirm our idea that the two-step synthesis method leads to nanometre-sized, crystalline metal oxide particles.

N_2-sorption isotherms were also recorded, in order to assess the porosity of the unsupported metal oxides (see Fig. 1(F)). Both show type II isotherms with a hysteresis loop, indicating a porous structure (presumably due to interparticle porosity). The surface areas calculated by the Brunauer–Emmett–Teller method are 60 and 148 m^2 g^{-1} for Co_3O_4 and $Fe_2O_3 \cdot$NCMs, respectively. These high surface areas are consistent with the porous structures, as shown by Fig. 2(B)).

The morphology and average particle size of the metal oxide NCMs are directly accessible from the TEM images shown in Fig. 2. For the AC-supported metal oxides obtained in the first step, the particles are very small and difficult to see in bright-field mode, therefore the dark-field mode was also used. Fig. 2(A) shows that the metal oxide particles are highly dispersed, and that the particle size is generally $\leqslant 5$ nm. A few large particles (<15 nm) are also present. They are attributed to concentration of the deposited metal ions on the support surface during the drying process, which is an unavoidable consequence of the impregnation method. After removal of the AC scaffold, agglomerated metal oxide nanoparticles are observed, however the small particle sizes from 5 to 10 nm show that they have not sintered to a larger extent. This is also seen by the porous morphology evident in Fig. 2B even after calcination at 500 °C for 2 h. This suggests that metal oxide NCMs prepared by this route have high thermal stability. The porous structure and small particle size are in agreement with those inferred by N_2-sorption isotherms and EXAFS (Fig. 1).

These results indicate that AC-supported metal oxide NCMs formed by heating in an inert atmosphere during the first synthesis step retain their structure when the AC support is removed in the second step. In order to demonstrate the advantage of prior metal oxide formation and immobilization by the two-step method, $Fe_2O_3 \cdot$NPs were also prepared using the one-step method (direct calcination of the supported metal nitrate) according to Schüth et al.[37] The product is denoted as "$Fe_2O_3\_NCM\_I$", and its properties are compared with those of $Fe_2O_3\_NCM\_II$ (prepared using the two-step method) in Table 1. Clearly, the latter has a higher surface area and pore volume, as well as a smaller particle size, indicating that immobilization in an inert atmosphere is indeed beneficial for the preparation of unsupported metal oxide NPs with

high surface area and porosity. Presumably decomposition of the nitrate ions in the absence of air limits the exotherm in the subsequent calcination step, as proposed by Schüth et al.[37] The resulting metal oxide NPs dispersed on AC are stable enough to resist agglomeration.

The high calcination temperature (500 °C) suggests that the NCMs may be robust enough for catalytic applications that require elevated temperatures, which represent a challenge for NCMs. Furthermore, the higher surface areas of metal oxides obtained using the two-step synthesis method described here should be beneficial for their catalytic activity. The catalytic performance of $Fe_2O_3\_NCM\_II$ was studied in CO oxidation, a reaction that is often required to operate at elevated temperatures.[44,45] For comparison, the catalytic performance of "$Fe_2O_3\_NCM\_I$" and an additional Fe_2O_3 sample prepared by an organic solution method without the AC scaffold (denoted as $Fe_2O_3\_Org$, see SI†) were also studied. The results are shown in Fig. 3.

Although the temperatures for onset of reactivity are similar for all three iron oxide catalysts (ca. 200 °C), the conversion increases most rapidly with temperature for $Fe_2O_3\_NCM\_II$, and at 330 °C, the CO_2 yield (100%) is far higher than for "$Fe_2O_3\_NCM\_I$" or $Fe_2O_3\_Org$ (both ca. 50%). Comparison of the TEM images for $Fe_2O_3\_NCM\_II$ before and after its use in CO oxidation shows no appreciable change in the particle size (Fig. S6†), confirming its stability as a high-temperature catalyst. Even more interesting, the $Co_3O_4 \cdot$NCMs show much better catalytic activity than $Fe_2O_3 \cdot$NCMs, to be discussed in our forthcoming work.

Conclusions

In summary, we have synthesized crystalline, nanometre-sized iron and cobalt oxides by a two-step method using activated carbon (AC) as a support/scaffold, resulting in particle sizes ranging from 5 to 10 nm and surface areas up to 148 m^2 g^{-1}. The metal oxide NCMs

Table 1 Comparison of the textural properties of $Fe_2O_3 \cdot$NPs, prepared by one- and two-step methods

Catalyst	S.A./m^2 g^{-1a}	P.V./cm^3 g^{-1b}	P.S./nm^c
$Fe_2O_3\_NCM\_II$	148	0.43	5–10
$Fe_2O_3\_NCM\_I$	59	0.28	~ 20

[a] Surface area determined by BET method (5-points). [b] Pore volume calculated at $p/p_0 = 0.99$. [c] Particle size evaluated from TEM images.
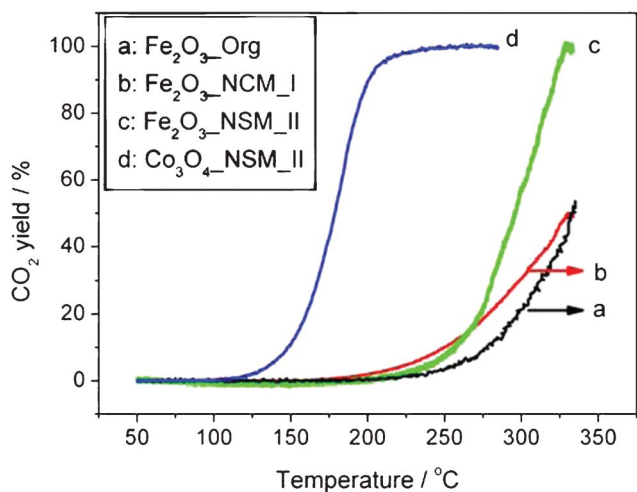
Fig. 3 Temperature-programmed reaction profiles for CO oxidation over three unsupported Fe_2O_3 catalysts, as well as over $Co_3O_4 \cdot NCMs$. Conditions: 0.4 vol% CO + 10 vol% O_2 in Ar; 50 mg catalyst; total flow rate 50 mL min^{-1}. Temperature ramp 5 °C min^{-1}.

persist at temperatures up to 500 °C without significant agglomeration, thus ensuring their stability under most reaction conditions. Furthermore, because the synthesis method described here is very simple, we expect it to be a general method for the preparation of metal oxide NCMs. The only requirement is that the metal precursor be soluble, so that it can be deposited on the AC support by wet impregnation.

Acknowledgements

References

1 M. M. Titirici, M. Antonietti and A. Thomas, *Chem. Mater.*, 2006, **18**, 3808.
2 J. R. A. Sietsma, J. D. Meeldijk, J. P. den Breejen, M. Versluijs-Helder, A. J. van Dillen, P. E. de Jongh and K. P. de Jong, *Angew. Chem., Int. Ed.*, 2007, **46**, 4547.
3 P. Poizot, S. Laruelle, S. Grugeon, L. Dupont and J. M. Tarascon, *Nature*, 2000, **407**, 496.
4 L. J. Zhi, Y. S. Hu, B. El Hamaoui, X. Wang, I. Lieberwirth, U. Kolb, J. Maier and K. Mullen, *Adv. Mater.*, 2008, **20**, 1727.
5 A. T. Bell, *Science*, 2003, **299**, 1688.
6 R. Schlogl and S. B. Abd Hamid, *Angew. Chem., Int. Ed.*, 2004, **43**, 1628.
7 W. Y. Li, L. N. Xu and J. Chen, *Adv. Funct. Mater.*, 2005, **15**, 851.
8 H. Cao and S. L. Suib, *J. Am. Chem. Soc.*, 1994, **116**, 5334.
9 S. O'Brien, L. Brus and C. B. Murray, *J. Am. Chem. Soc.*, 2001, **123**, 12085.
10 M. Haruta, *Catal. Today*, 1997, **36**, 153.
11 M. Haruta, *CATTECH*, 2002, **6**, 102.
12 G. J. Hutchings and M. Haruta, *Appl. Catal., A*, 2005, **291**, 2.
13 A. Murali, A. Barve, V. J. Leppert, S. H. Risbud, I. M. Kennedy and H. W. H. Lee, *Nano Lett.*, 2001, **1**, 287.
14 Y. D. Wang, C. L. Ma, X. D. Sun and H. D. Li, *Inorg. Chem. Commun.*, 2002, **5**, 751.
15 X. L. Xu, J. D. Guo and Y. Z. Wang, *Mater. Sci. Eng., B*, 2000, **77**, 207.
16 S. Castro-Garcia, S. Yanez-Vilar, M. Sanchez-Andujar, C. Gomez-Aguirre, J. Mira and M. A. Senaris-Rodriguez, *J. Solid State Chem.*, 2009, **182**, 2685.
17 X. H. Liu, A. Yan, G. Qiu, N. Zhang, R. R. Shi, R. Yi, M. Tang and R. C. Che, *Solid State Commun.*, 2007, **144**, 315.
18 V. Polshettiwar, B. Baruwati and R. S. Varma, *ACS Nano*, 2009, **3**, 728.
19 B. H. Wu, Y. J. Kuang, X. H. Zhang and J. H. Chen, *Nano Today*, 2011, **6**, 75.
20 J. H. He, T. Kunitake and A. Nakao, *Chem. Mater.*, 2003, **15**, 4401.
21 Y. W. Tan, X. H. Dai, Y. F. Li and D. B. Zhu, *J. Mater. Chem.*, 2003, **13**, 1069.
22 C. L. Lee, C. C. Wan and Y. Y. Wang, *Adv. Funct. Mater.*, 2001, **11**, 344.
23 J. J. Zhu, X. Xie, S. A. C. Carabineiro, P. B. Tavares, J. L. Figueiredo, R. Schomaecker and A. Thomas, *Energy Environ. Sci.*, 2011, **4**, 2020.
24 F. Rodriguez-Reinoso, *Carbon*, 1998, **36**, 159.
25 M. D. Hughes, Y. J. Xu, P. Jenkins, P. McMorn, P. Landon, D. I. Enache, A. F. Carley, G. A. Attard, G. J. Hutchings, F. King, E. H. Stitt, P. Johnston, K. Griffin and C. J. Kiely, *Nature*, 2005, **437**, 1132.
26 D. S. Su, J. Zhang, B. Frank, A. Thomas, X. C. Wang, J. Paraknowitsch and R. Schlogl, *ChemSusChem*, 2010, **3**, 169.
27 J. L. Figueiredo and M. F. R. Pereira, *Catal. Today*, 2010, **150**, 2.
28 M. L. Toebes, F. F. Prinsloo, J. H. Bitter, A. J. van Dillen and K. P. de Jong, *J. Catal.*, 2003, **214**, 78.
29 L. Prati and G. Martra, *Gold Bull.*, 1999, **32**, 96.
30 L. Prati and M. Rossi, *J. Catal.*, 1998, **176**, 552.
31 J. J. Zhu, K. Kailasam, A. Fischer and A. Thomas, *ACS Catal.*, 2011, **1**, 342.
32 J. J. Zhu, J. L. Faria, J. L. Figueiredo and A. Thomas, *Chem.–Eur. J.*, 2011, **17**, 7112.
33 H. J. Fan, Q. Xu, Y. Q. Guo, Q. Peng and Z. Z. Hou, *Mater. Sci. Eng., A*, 2006, **422**, 272.
34 H. J. Fan, Q. Xu, J. G. Li and Y. X. Cao, *J. Am. Ceram. Soc.*, 2006, **89**, 3065.
35 W. Rarog-Pilecka, E. Miskiewicz and Z. Kowalczyk, *Catal. Commun.*, 2008, **9**, 870.
36 H. N. Yang, L. F. Liu, F. L. Yang and J. C. Yu, *J. Zhejiang Univ., Sci., A*, 2008, **9**, 981.
37 M. Schwickardi, T. Johann, W. Schmidt and F. Schüth, *Chem. Mater.*, 2002, **14**, 3913.
38 S. A. C. Carabineiro, S. S. T. Bastos, J. J. M. Orfao, M. F. R. Pereira, J. L. Delgado and J. L. Figueiredo, *Appl. Catal., A*, 2010, **381**, 150.
39 S. A. C. Carabineiro, S. S. T. Bastos, J. J. M. Orfao, M. F. R. Pereira, J. J. Delgado and J. L. Figueiredo, *Catal. Lett.*, 2010, **134**, 217.
40 B. Ernst, A. Bensaddik, L. Hilaire, P. Chaumette and A. Kiennemann, *Catal. Today*, 1998, **39**, 329.
41 F. Jiao, A. Harrison, J. C. Jumas, A. V. Chadwick, W. Kockelmann and P. G. Bruce, *J. Am. Chem. Soc.*, 2006, **128**, 5468.
42 T. Liu, L. Guo, Y. Tao, T. D. Hu, Y. N. Xie and J. Zhang, *Nanostruct. Mater.*, 1999, **11**, 1329.
43 M. Kitagami, T. Konishi, T. Kaneko, M. Sakamaki, L. Lin, J. G. Lin, D. Arvanitis and T. Fujikawa, *Photon Factory Activity Report 2006 #24 Part B*, 2007, 12C/2006G356.
44 Y. H. Zheng, Y. Cheng, Y. S. Wang, F. Bao, L. H. Zhou, X. F. Wei, Y. Y. Zhang and Q. Zheng, *J. Phys. Chem. B*, 2006, **110**, 3093.
45 P. Li, D. E. Miser, S. Rabiei, R. T. Yadav and M. R. Hajaligol, *Appl. Catal., B*, 2003, **43**, 151.